Inorganic Chemistry
Cite This: Inorg. Chem. 2019, 58, 15487−15497
Article
pubs.acs.org/IC

Unsymmetrical Bis-Alkynyl Complexes Based on Co(III)(cyclam): Synthesis, Ultrafast Charge Separation, and Analysis

Susannah D. Banziger,[†,#] Xiao Li,[‡,#] Jesús Valdiviezo,[§] Matthias Zeller,[†] Peng Zhang,[§] David N. Beratan,[*,§,∥,⊥] Igor V. Rubtsov,[*,‡] and Tong Ren[*,†]

[†]Department of Chemistry, Purdue University, West Lafayette, Indiana 47907, United States
[‡]Department of Chemistry, Tulane University, New Orleans, Louisiana 70118, United States
[§]Department of Chemistry, Duke University, Durham, North Carolina 27708, United States
[∥]Department of Physics, Duke University, Durham, North Carolina 27708, United States
[⊥]Department of Biochemistry, Duke University, Durham, North Carolina 27710, United States

Supporting Information

ABSTRACT: Donor-bridge-acceptor (D-B-A) systems with a polarizable bridge can afford rapid photoinduced electron transfer dynamics that may be susceptible to rate modulation by infrared excitation. We describe the synthesis, characterization, and electronic structure of a class of readily assembled D-B-A structures linked by a cobalt cyclam bridge. The reaction between $[Co(cyclam)Cl_2]Cl$ and 4-ethynyl-*N*-isopropyl-1,8-naphthalimide (HC_2NAP^{iPr}) yields $[Co(cyclam)(C_2NAP^{iPr})Cl]Cl$ (**1**), which reacts with LiC_2Y at −78 °C to afford $[Co(cyclam)(C_2NAP^{iPr})(C_2D)]Cl$ with D as C_6H_4-4-NMe_2 (**2a**), NAP^{iPr} (**2b**), Ph (**2c**), and C_6H_4-4-N(4-MeOPh)$_2$ (**2d**). Molecular structures of **1** and **2a** were established using single-crystal X-ray diffraction, while the redox properties and fluorescence profiles of compounds **1** and **2** were examined using voltammetric and steady-state emission techniques, respectively. The electronic structures and photophysical properties of these compounds were studied using density functional theory and time-dependent density functional theory methods. The excited-state dynamics of compounds **1**, **2a**, and **2d** were explored using femtosecond transient absorption spectroscopy with 400 nm excitation and detection in both the visible and mid-IR spectral regions. Formation of a long-lived excited state was complete within 20 ps of excitation in all three compounds. Ultrafast spectral changes observed in **2a** and **2d** within the first 20 ps indicated the formation of a charge separated state (CS state, D^+-B-A^-) with characteristic times of less than 0.1 and 0.25 ps, respectively. The CS state undergoes rapid charge recombination (8 ps in **2a** and 4 ps in **2d**). The CS dynamics is facilitated by the Co center, which mixes the bright NAP-centered electronic state with a pure CS state. The mixing strength depends on the donor energetics and conformation, which significantly influences the charge transfer dynamics in **2a** and **2d**.

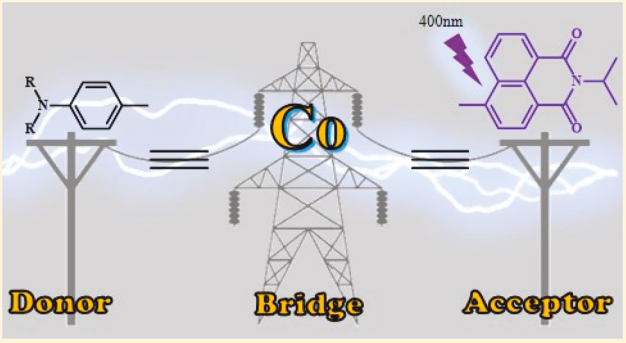

INTRODUCTION

Molecular donor-bridge-acceptor (D-B-A) structures have received intense interest as electron-transfer (ET) model systems.[1,2] A topic of recent notice is the modulation of ET dynamics through vibrational excitation. Studies of this kind require ultrafast ET that proceeds more rapidly than intramolecular vibrational energy redistribution. As such, strongly coupled D-B-A structures with infrared (IR) active bridge modes are a key synthetic target.

Rubtsov, Beratan, Sessler, and co-workers demonstrated charge separated (CS) rate retardation by mid-IR excitation in a D-B-A ensemble formed by nucleobase pairing (GC)[3] and charge recombination (CR) rate acceleration upon mid-IR excitation.[4] They related the rate modulations to the changes in the density of states in the Marcus curve-crossing region.[4] Rubtsov, Schmehl, Beratan, and co-workers also reported a ca. 30% enhancement of intramolecular ligand-to-ligand charge transfer (CT) rate in a Re(I) compound via selective excitation of the acceptor ligand 4,4′-(dicarboxyethyl)-2,2-bipyridine at 1540 cm^{-1} (ν(bpy)).[5] Weinstein and co-workers studied a series of D-B-A compounds with a *trans*-Pt(II)-bis-alkynyl bridge and found that the photoinduced electron transfer (PET) between phenothiazine (donor (D)) and naphthalimide (acceptor (A)) can be attenuated by vibrational excitation of the Pt-bound C≡C bonds.[6−9]

Transition-metal alkynyl compounds are appealing targets from the standpoints of synthetic and structural chemistry, as well as materials applications, and could provide access to species with rapid intramolecular ET rates that may be

Received: August 24, 2019
Published: November 7, 2019

DOI: 10.1021/acs.inorgchem.9b02557
Inorg. Chem. 2019, 58, 15487−15497

susceptible to IR-induced rate modulation.[10−13] Materials applications of transition-metal alkynyl compounds include molecular wires,[14−17] molecular memory devices,[18,19] and high-performance optoelectronic materials.[20−23] Recently, metal alkynyl compounds based on 3d metal cyclams have been investigated by Ren and co-workers.[24,25] The Co(III)-(cyclam) motif is especially attractive because of the feasibility of stepwise alkynylation under mild reaction conditions. This was first demonstrated by Shores and co-workers through the preparation of $[Co(cyclam)(C_2Ph)Cl]^+$,[26] and it was explored by the Ren group to attain the dicobalt complexes bridged by oligoyn-diyls (μ-C_{2m}).[27,28] The general preparations of the unsymmetric *trans*-$[Co(cyclam)(C_2Ar)(C_2Ar')]^+$ compounds were developed either through an intermediate *trans*-$[Co(cyclam)(C_2Ar)(NCCH_3)]^{+2}$,[29,30] or via lithiation to install the second alkyne.[31] Such Co(III) bis-alkynyls are attractive alternatives to the aforementioned Pt species, since the Co species also provide a rigid framework for D-B-A dyads, and the structures possess vibrationally active Co−C≡C bonds based on an earth abundant metal.

The transient absorption studies of Co(III)-containing complexes are scarce, and studies of cobalamin species focused on the effects Co−C bonds are noteworthy.[32,33] Transient absorption studies of electronically excited Co complexes show complexity in the dynamics, with characteristic times ranging from a few picoseconds to a few nanoseconds.[34,35] The ligand-field (LF) excited states in octahedral Co(III) complexes were found to occur at energies below 12 000 cm^{-1}.[34] Nevertheless, the lifetime of the lowest electronic excited state (ES) in some species, such as $[Co(en)_3](ClO_4)_3$ (en = ethylenediamine), $[Co(tpen)](ClO_4)_3$ (tpen = tetrakis(2pyridylmethyl)-ethylenediamine), $[Co(tppn)](ClO_4)_3$ (tppn = tetrakis(2-pyridylmethyl)-1,2-propylenediamine), $[Co(NH_3)_5Cl]^{2+}$, and $[Co(en)_2(NO_2)_2Cl]^{2+}$, were found to be rather short, not exceeding 500 ps.[34,36]

Here, we report the synthesis of *trans*-$[Co(cyclam)(C_2D)-(C_2A)]^+$ complexes, where D and A are C_6H_4-4-Y (Y = H, NMe_2, or N(4-MeOPh)$_2$) and *N*-isopropyl-1,8-napthalimide (NAP^{iPr}), respectively, Scheme 1, along with the structural,

Scheme 1. Synthetic Approach towards Co^{III}(cyclam)-Based D-B-A

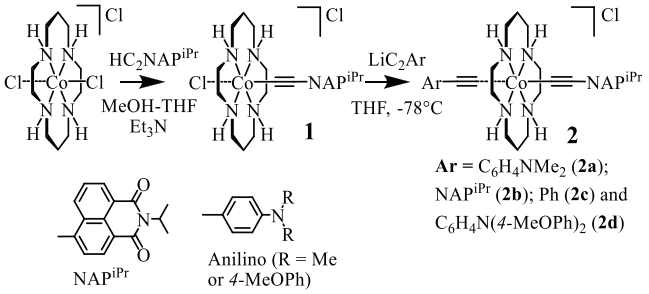

spectroscopic, voltammetric, and electronic structure properties of these compounds. The excited-state dynamics of compounds **1**, **2a**, and **2d** were examined using femtosecond transient absorption spectroscopy with 400 nm excitation and detection both in the visible and mid-IR spectral regions. The dynamics reveal the ultrafast formation of charge separated states (CS state) in compounds **2a** and **2d** and their fast conversion to a Co(III) centered triplet state ($^3T_1$). Our study also finds that the MN15 density functional, a functional optimized using databases that included transition metals, describes the excited-state properties of Co(III) complexes, especially the charge transfer excitation energies, a task that is challenging for most functionals.

RESULTS AND DISCUSSION

Synthesis. As shown in Scheme 1, the Co^{III}(cyclam)-based D-B-A complexes were prepared in a stepwise fashion. 4-Ethynyl-*N*-isopropyl-1,8-naphthalimide (HC_2NAP^{iPr})[37] and 4-ethynyl-*N*,*N*-bis(4-methoxyphenyl)aniline (HC_2TPA)[38] (TPA = -C_6H_4-4-N(Ph-4′-OMe)$_2$) were prepared according to literature methods. $[Co(cyclam)(C_2NAP^{iPr})Cl]Cl$ (**1**) was prepared under N_2 through the reaction of HC_2NAP^{iPr}, and $[Co(cyclam)Cl_2]Cl$ was prepared under weak base conditions (see a general review for weak base promoted dehydrohalogenation alkynylation[39]) to produce an orange microcrystalline solid in 87% yield after purification using a silica column. Synthesis of $[Co(cyclam)(C_2NAP^{iPr})(C_2C_6H_4$-4-$NMe_2)]Cl$ (**2a**) was accomplished in a yield of 50% via addition of 1.2 equiv of $LiC_2C_6H_4$-4-NMe_2 to **1** at −78 °C. Symmetric $[Co(cyclam)(C_2NAP^{iPr})_2]Cl$ (**2b**) was prepared similarly in 37% yield as were complexes $[Co(cyclam)(C_2NAP^{iPr})(C_2Ph)]Cl$ (**2c**) and $[Co(cyclam)(C_2NAP^{iPr})(C_2TPA)]Cl$ (**2d**) in yields of 26% and 19%, respectively. Compounds containing an electron-donating substituent (**2a** and **2d**) are light orange solids, while compounds **2b** and **2c** are bright yellow solids. All compounds presented herein are low-spin Co(III) species, and they are readily characterized using ^1H NMR, UV−vis, and FT-IR spectroscopies, electrospray ionization mass spectrometry, and combustion analysis.

Structure Analysis. Molecular structures of complexes **1** and **2a**, determined using single-crystal X-ray diffraction, are shown in Figures 1 and 2, respectively, while selected bond

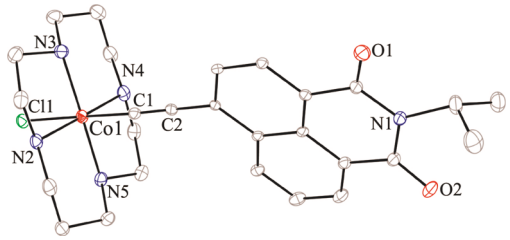

Figure 1. Molecular structure of the cation in **1** at 30% probability level; counterions, hydrogen atoms, and solvent molecules were omitted for clarity. Selected bond lengths (Å): Co1−C1 1.888(4), Co1−Cl1 2.3314(2), C1−C2 1.206(5), Co−N_{av} 1.976[4].

lengths and angles are found in Supporting Information (Table S1). Both compounds are in pseudo-octahedral configurations with the cyclam ring in the *XY* plane and alkynyl/chloro ligands occupying the axial positions (*Z* axis). The lengths of the C≡C bonds were within the expected range of metal alkynyl species,[12] as were the Co−C distances for both **1** and **2a**. Consistent with the previous structural analysis, the Co−C bond distances in bis-alkynyl species **2a**, 1.932(3) and 1.925(3)Å, are longer than that of monoalkynyl species **1** (1.888(4)Å), and the elongation can be attributed to the greater *trans*-influence in **2a**, thereby resulting in longer Co−C bond lengths.[28,29,31,40] The donor and acceptor aromatic rings are separated, through bond, by 9.177 Å (C3−C20) with a dihedral angle between the donor and acceptor ligand planes of ∼60° in **2a** (Figure 2).

DOI: 10.1021/acs.inorgchem.9b02557
Inorg. Chem. 2019, 58, 15487−15497

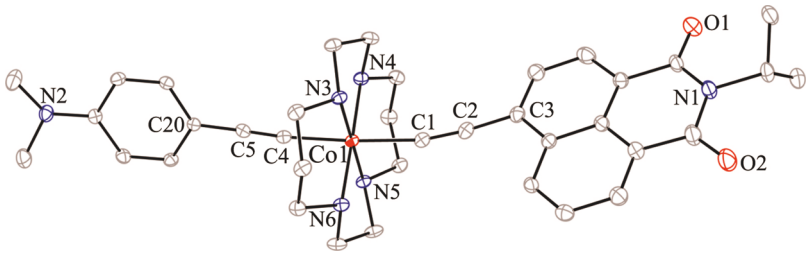

Figure 2. Molecular structure of the cation in **2a** at 30% probability level; counterions, hydrogen atoms, and solvent molecules were omitted for clarity. Selected bond lengths (Å): Co1−C1 1.932(3), Co1−C4 1.925(3), C1−C2 1.223(4), C4−C5 1.208(4), Co−N_{av} 1.986[2], C3−C20 9.177 Å.

Electrochemistry. The redox profiles of the Co^{3+}(cyclam) complexes were examined using cyclic voltammetry. The resultant cyclic voltammograms (CVs) for **1**, **2a**, **2b**, and **2d** are shown in Figure 3, and CVs showing Co-based reduction

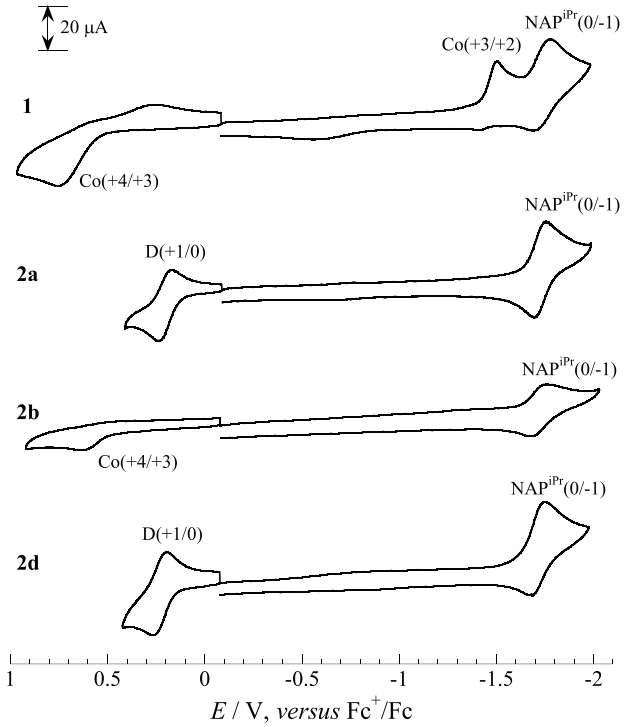

Figure 3. CVs of compounds **1**, **2a**, and **2d** recorded in 1.0 mM solutions CH_3CN solutions with 0.1 M *n*-Bu_4NPF_6 as the supporting electrolyte. Because of the low solubility of **2b**, its CV was recorded in a 0.22 mM solution.

couples are provided in Figure S1. The electrode potentials for all five complexes are collected in Table 1. Consistent with previous studies of the $[Co(cyclam)(C_2R)Cl]^+$ complexes,[25] **1** displays one irreversible 1e$^-$ oxidation ($Co^{4+/3+}$), an irreversible 1e$^-$ reduction on Co ($Co^{3+/2+}$), and a reversible 1e$^-$ reduction localized on NAP^{iPr}. For the D-B-A dyads **2a** and **2d**, the cyclic voltammograms feature quasi-reversible 1e$^-$ reduction and 1e$^-$ oxidation that are ascribed to NAP^{iPr} and the N-donor (free ligand electrode potentials listed in Table 1), respectively, from which the electrochemical highest occupied molecular orbital (HOMO)−lowest unoccupied molecular orbital (LUMO) gap ($E_g = E_{1/2}(D) - E_{1/2}(A)$) is calculated as 1.90 (**2a**) and 1.94 (**2d**) eV. Upon addition of the second alkynyl, the $Co^{3+/2+}$ reduction couple is cathodically shifted by ∼0.62 V (Table 1), significantly more negative than

Table 1. Electrode Potentials of All Observed Redox Couples (V) in 1 and 2a−2d[a]

	$E_{1/2}$ (D)	$E_{1/2}$ (A)	E_{pc} ($Co^{3+/2+}$)	E_{pc} ($Co^{2+/1+}$)
1		−1.74 (0.09)	−1.49	−2.25
2a	0.21 (0.09)	−1.69 (0.06)	−2.11	−2.32
2b		−1.72 (0.08)	−2.14	−2.26
2c[b]		−1.72 (0.06)	−2.09	−2.25
2d	0.23 (0.07)	−1.71 (0.07)	−2.11	−2.33
HC_2NAP^{iPr} [b]		−1.58 (0.07)		
$HC_2C_6H_4$-4-NMe_2[b,c]	0.43			
HC_2TPA[b,c]	0.30 (0.07)			

[a]Potentials vs Fc^+/Fc collected in CH_3CN solutions at a scan rate of 100 mV/s with 0.1 M *n*-Bu_4NPF_6 as the supporting electrolyte; peak separation (ΔE_p) for reversible processes shown in brackets. [b]CV included in the Supporting Information Figures S1 and S2. [c]CVs collected in CH_2Cl_2.

that of NAP^{iPr}. This trend is attributed to increased electron density at the Co center for the bis-alkynyl species.[25] On the basis of the comparison of the currents of the NAP^{iPr} reduction in **1** and **2b** (Figure 3) and considering the concentration of the latter being less than one-fourth of the former, **2b** undergoes a quasi-reversible 2e$^-$ reduction, that is, simultaneous reduction of both NAP^{iPr} groups. It is noteworthy that the reduction potentials of NAP^{iPr} are within a very narrow range for both mono- and bis-acetylide species. Similarly, the reduction of the NAP^{iPr} group was consistently measured at −1.83 V versus ferrocene in CH_2Cl_2 for the Pt(II)-based *trans*-acetylide donor−bridge−acceptor species,[8] and the difference in $E_{1/2}$ between the Co(III) and Pt(II) complexes is attributed to the difference in the solvents used.

UV−Vis Spectroscopic Analysis. Absorption spectra for complexes **1** and **2a−2d** are shown in Figure 4. For all of the complexes, the visible window is dominated by a broad and intense peak at ca. 400 nm. The free ligand $Me_3SiC_2NAP^{iPr}$ displays an intense peak at ca. 370 nm (see Figure S3 in Supporting Information), which is assigned as a $\pi-\pi^*$ transition localized on NAP^{iPr}. The strong resemblance of the spectral shapes and extinction coeffcients for complexes **1** and **2** and $Me_3SiC_2NAP^{iPr}$ suggests that the transition at 400 nm is primarily a $\pi-\pi^*$ transition localized on NAP^{iPr}. This assignment is supported by time-dependent density functional theory (TD-DFT) analysis (vide infra). The 30 nm red shift of the transition from $Me_3SiC_2NAP^{iPr}$ to the values in complexes **1** and **2** is apparently due to the replacement of Me_3Si with a Co(III) center. The broad nature of the 400 nm peak obscures the expected d−d ($^1A_1 \rightarrow {}^1T_1$) transition, except in the case of **1**, where a weak shoulder peak is observed around 480 nm,

DOI: 10.1021/acs.inorgchem.9b02557
Inorg. Chem. 2019, 58, 15487−15497

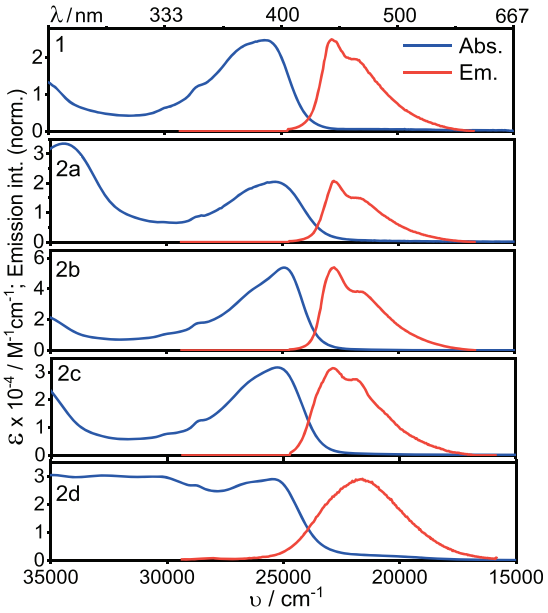

Figure 4. UV−Vis absorption spectra in CH_2Cl_2 vs normalized emission spectra in CH_2Cl_2, taken at room temperature, for **1** and **2a**−**2d**.

consistent with values reported for other Co(cyclam) bisalkynyls.[41] The D-B-A species **2a** and **2d** display UV bands attributed to the donor ligands. Compound **2a** displays a sharp peak at 290 nm, which can be assigned to a π−π^* transition localized on C_6H_4-4-NMe_2, and compound **2d** has a broad band centered at 330 nm assigned to a π−π^* transitions localized on TPA (Figure 4). This is consistent with the absorption spectrum of the free donor ligands, which exhibit a strong absorption ca. 300 nm (Figure S4). Note that no such peak is present for **2b** or **2c**, due to the absence of an N-donor aryl substituent.

To understand the nature of the transition with high oscillator strength at ca. 400 nm, TD-DFT calculations of compounds **1**, **2a**, and **2d** were performed. The analysis indicates that the bright state involves only NAP^{iPr} orbitals in **1** (Figure S5), but that the states are partially polarized in **2a** and **2d**, involving ca. 8.4% contribution of the orbitals responsible for CS (i.e., the HOMO of the donor (D(HOMO)) and the LUMO of the acceptor (A(LUMO), Figures 5 and S7). The percentages reflect the normalized squared excitation coefficients. To evaluate the amount of CT character in the transition, the dipole moments were evaluated for both the ground and excited states. The ground states are found to be polarized, with the NAP^{iPr} acceptor having a slight negative charge (Table S3). The dipole moments are further increased in the excited states by ca. 5.6, 25.2, and 10.5 D for **1**, **2a**, and **2d**, respectively.

Emission Studies. Steady-state emission studies found that **1** and **2a**−**2c** exhibit similar profiles with the emission maxima (λ_{em}) within a narrow range of 437−439 nm, which are red-shifted from λ_{em} of the free ligand (401 nm), as shown in Figure 4. The mirror image relation between the absorption and emission spectra, and the reasonably small Stokes shifts, suggest that the observed emission occurs from the same excited state prepared by 400 nm excitation. The emission maximum of **2d** is more red-shifted compared to those of **2a**−**2c**, hinting at a stronger influence of the TPA donor on NAP^{iPr}. Emission quantum yields were measured for each metal

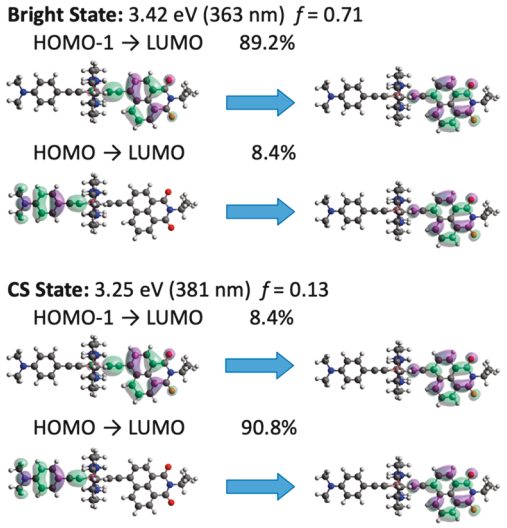

Figure 5. TD-DFT analysis showing orbital transitions that contribute to the bright excited state prepared with a 400 nm pump (bright state) and the CS state for **2a**. A mixing between the HOMO−1 → LUMO and HOMO → LUMO transition is present in both states. The high oscillator-strength transition is mainly a π−π^* transition localized on NAP^{iPr}(89.2%), and the CS state is mostly D(HOMO) → A(LUMO) (90.8%). The transition energies and wavelengths of these states are blue-shifted with respect to the experimental values (ca. 30 nm), which is generally found in TD-DFT analysis. The oscillator strength (f) values, which indicate the probability of absorbing a photon, are also indicated.

Table 2. Absorption and Emission Maxima (λ/nm) and Emission Quantum Yields (Φ) in CH_2Cl_2

	Φ_{fl}	λ_{abs}	λ_{em}	λ_{ex}
1	0.0066	388	438	390
2a	0.0068	401	439	400
2b	0.0143	395	439	400
2c	0.0043	397	437	400
2d	0.026	393	461	320
	0.00063			400

complex and the NAP^{iPr} ligand (Table 2). The bridging metal center significantly reduces the fluorescence quantum yield (Φ_{fl}) of metal-bound NAP^{iPr} in comparison with that of HC_2NAP^{iPr} (0.423). Compound **2b** features two NAP^{iPr} groups and has Φ_{fl} of 0.0143, which is approximately twofold larger than the yields for **1**, **2a**, and **2c** (Table 2). Such doubling, associated with the presence of two NAP^{iPr} groups in **2b**, indicates independent behavior of the two NAP^{iPr} ligands in **2b**. Φ_{fl} for **2d** depends strongly on excitation energy (Table 2): it is ∼0.026 when excited at 320 nm (TPA) and drops precipitously to 0.0006 when excited at 400 nm (NAP^{iPr}). Note that these Φ_{fl} values are significantly lower than the quantum yields reported for Pt-bridged D-B-A species by the Weinstein group, which were ca. 0.055,[8] suggesting faster excited-state relaxation in **2a** and **2d** compared to the Pt compounds. The observed quantum yields are similar to those of ferrocenyl naphthalimide donor−acceptor complexes bridged by a single alkyl carbon, with quantum yields ≈ 0.002, where the fluorophore quenching was attributed to the ferrocene redox center.[42] High-energy excitation of **2d** significantly involves the donor moiety, resulting in a higher emission quantum yield. This observation suggests that the

DOI: 10.1021/acs.inorgchem.9b02557
Inorg. Chem. 2019, 58, 15487−15497

formation of the CS state is suppressed under these conditions, but no detailed explanation can be provided at this time.

The ES decay rate in complexes **1** and **2** can be roughly estimated by assuming that the radiative rate of NAP^{iPr} (k_{rad}) in complexes **1** and **2** is similar to those in compounds without Co (HC_2-NAP^{iPr} or $Me_3SiC_2-NAP^{iPr}$), which is ca. $(1\ ns)^{-1}$, computed as Φ_{fl} divided by its ES lifetime of 0.5 ns. The ES lifetime in **2a** is then approximately $\Phi_{fl}/k_{rad} = 0.0068 \times 1\ ns \approx 7$ ps, suggesting a characteristic time scale for observing CS in **2a**.

Fourier Transform IR (FT-IR) Spectroscopy. The IR absorption spectra of **1**, **2a**, and **2d** are dominated by the antisymmetric ($\nu_{C=O,as}$) and symmetric ($\nu_{C=O,ss}$) C=O stretching modes of NAP^{iPr} at 1658 and 1698 cm^{-1} in **1** and 1656 and 1697 cm^{-1} in **2a** and **2d** (Figure 6). The C≡C stretching frequencies in **2a** and **2d** (2092 cm^{-1}) are significantly red-shifted compared to compound **1** (2110 cm^{-1}), indicating the influence of the donor moieties.

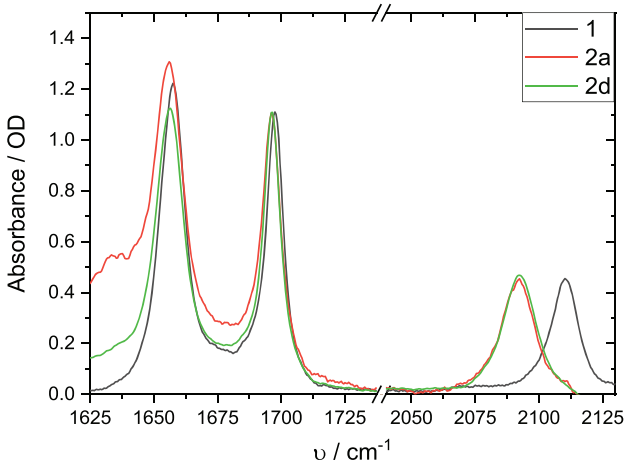

Figure 6. IR absorption spectra of **1**, **2a**, and **2d** in CH_3CN.

DFT-based normal-mode analysis finds that the two C≡C vibrations in the ground states of **2a** and **2d** are coupled weakly with an interaction energy of a few wavenumbers, while the frequencies of the normal modes are separated by ca. 18 cm^{-1} with the low-frequency peak originating predominantly from the donor acetylide and the high-frequency peak from the acceptor acetylide. Essentially, a single peak is observed experimentally with a weak tail on the high-frequency side, in approximate agreement with the DFT analysis, which predicts that the lower-frequency peak carries ca. fourfold larger IR intensity (Table S4). The extinction coefficients of the C=O and C≡C modes in the three compounds are similar but grow with increasing donor strength, with $\varepsilon_{C=O,ss}$ of 1230, 1360, and 1475 $M^{-1}\ cm^{-1}$ for **1**, **2a**, and **2d**, respectively. The transition dipoles of the C=O and C≡C modes grow concomitantly in the three compounds, which is apparent from the essentially unchanged extinction coefficient ratio of $\nu_{C=O,ss}$ and $\nu_{C\equiv C}$ of ca. 2.4 (Figure 6).

Time-Resolved Spectroscopy in the Visible and Infrared Regions. Transient absorption spectra of compounds **1**, **2a**, and **2d** in the visible and mid-IR regions are shown in Figures 7 and 8. In the visible region, a pronounced excited-state absorption (ESA) is observed in the 450−730 nm window for all three compounds (Figure 7). Within the first 20 ps after excitation the spectral evolution is rather small in **1** but

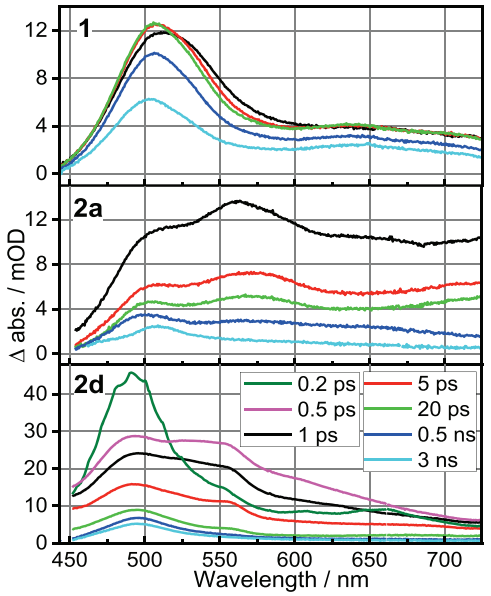

Figure 7. Transient absorption spectra for **1**, **2a**, and **2d** in CH_3CN in the visible region at the time delays indicated in the inset. λ_{pump} = 400 nm.

significant in **2a** and very large in **2d**, occurring with characteristic times of 0.2−8 ps. The spectral changes are essentially completed within 20 ps. The transient spectra measured at 20 ps delay have similar shapes for all three compounds with the peaks at ca. 500 and 650 nm; these spectra decay concomitantly to zero absorbance with long decay times of 2.0 (**1**), 3.3 (**2a**), and 4.0 ns (**2d**), suggesting that the transition to the ground state is spin-forbidden. Note that the stimulated emission (^{1}NAP) *may* contribute to transient absorption signal at 400 < λ, nm < 500, though its contribution at λ > 450 nm (measured region) is smaller than the ESA for all three compounds.

To help understand the excited-state dynamics, the transient spectra in the mid-IR region were measured (Figure 8). At small delay times, several ground-state bleach (GSB) peaks were found in the transient spectra of each compound, matching the vibrational peaks in the ground electronic state (Figure 8, gray lines). The ESA peaks of two carbonyl stretching modes of NAP (below, NAP is used in place of NAP^{iPr} for the sake of brevity), $\nu_{C=O,ss}$ and $\nu_{C=O,as}$, are very broad and shifted to lower frequencies in all three compounds compared to the ground-state absorption (Figure 8a). The ESA peaks decay rapidly in all three compounds with characteristic times ranging from 0.2 to 8 ps. These kinetic steps do not populate the ground states but result in formation of the long-lived states (LLS), as also observed in the transient spectra in the visible range (Figure 7). We will demonstrate below that the peak at ca. 550 nm is characteristic for ESA of the CS state. The carbonyl frequencies in this LLS are blue-shifted by a few wavenumbers relative to those in the GS resulting in cancellation of the GSB and ESA C=O peaks and formation of characteristic, distinctive transient spectra with negative peaks at the red side of the GS peaks and positive peaks on the blue side (Figure 8a, $t \geq 20$ ps). The long-lived species decay with nanosecond decay times, matching those measured in the visible region. Essentially no GS recovery is observed in the three compounds at early times, as apparent from persistence of the GSB peaks of $\nu_{C\equiv C}$ (Figure 8b), which

DOI: 10.1021/acs.inorgchem.9b02557
Inorg. Chem. 2019, 58, 15487−15497

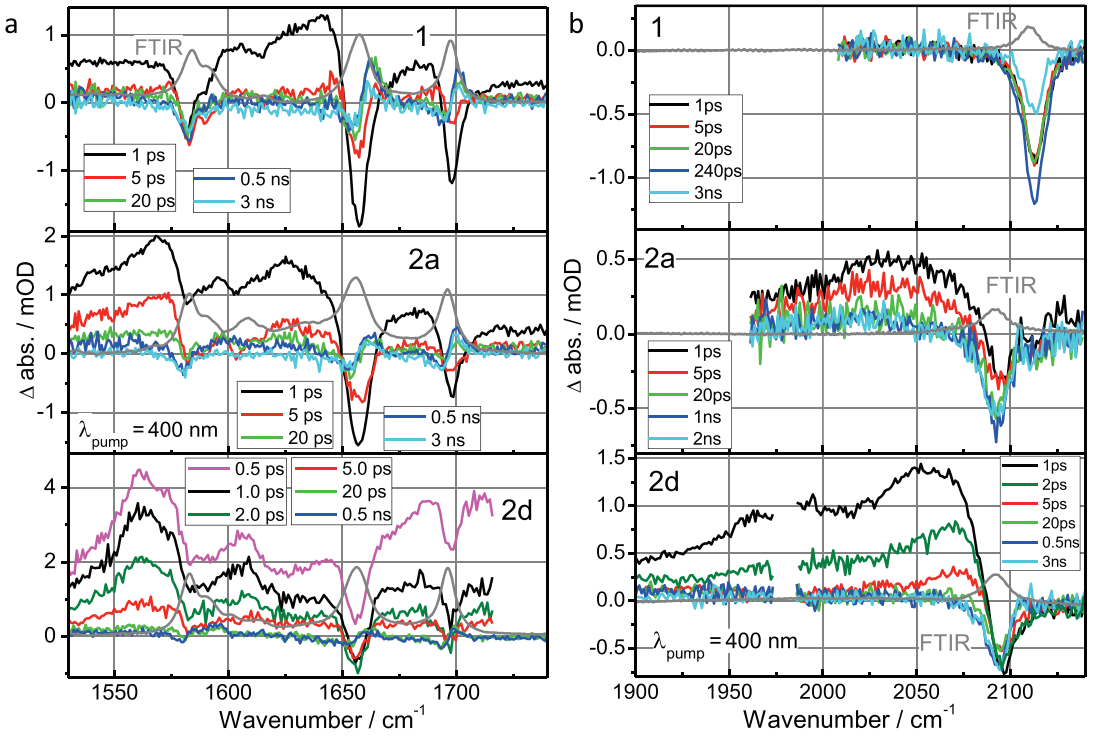

Figure 8. Transient absorption spectra for **1**, **2a**, and **2d** in CH_3CN in the (**a**) 1500−1740 cm^{-1} and (**b**) 1900−2130 cm^{-1} mid-IR regions. The time delays are indicated as insets.

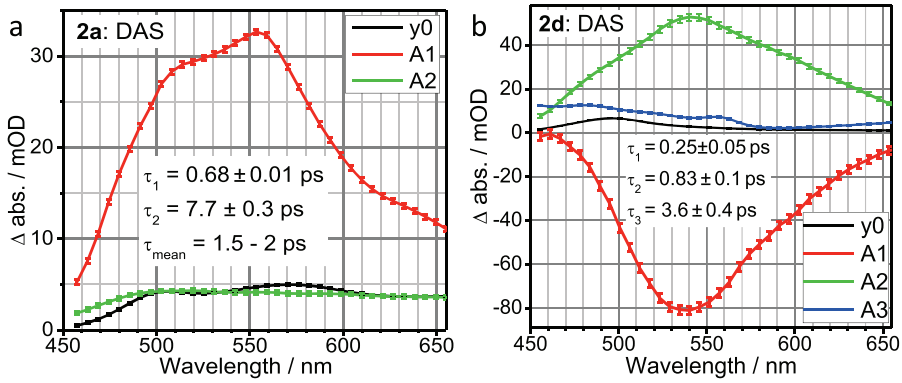

Figure 9. Decay-associated spectra for **2a** (a) and **2d** (b) constructed for the spectral dynamics within 60 ps window.

decay with nanosecond times, also matching the slow decay component in the visible region.

The transient spectra of the $\nu_{C\equiv C}$ modes differ considerably for the three compounds (Figure 8b). For **1**, the $\nu_{C\equiv C}$ ESA is negligible, suggesting that the initial excited state of **1** is weakly polarized. The $\nu_{C\equiv C}$ ESA peaks in **2a** and **2d** are significantly stronger than the respective GSB peaks, with the square of the transition dipole ratios, $\mu^2_{(ES)}/\mu^2_{(GS)}$, of 5 and 9, respectively, indicating formation of the states that are strongly polarized across the bridge, involving charge transfer from donor to acceptor. In agreement with the measured visible region transient spectra, formation of the LLS in all three compounds, which is detected in the mid-IR, is completed in 20 ps. To characterize the CS state formed in **2a** and **2d**, two spectral features in the transient IR spectra were used: (i) the strong absorption of $\nu_{C=O}$ for the NAP anion, occurring at ca. 1570−1580 cm^{-1} (Figure 8a)[43] and (ii) the broad absorption of $\nu_{C\equiv C}$ (1930−2100 cm^{-1}, Figure 8b), which reports the CS state dynamics. Both indicators suggest formation of the CS state in **2a** and **2d**, while two peaks are significantly stronger in **2d**.

TD-DFT analysis indicates that the CS state in **2d** (Figure S7) is essentially a pure charge transfer transition, involving 97.2% D(HOMO) → A(LUMO) orbitals, while in **2a** (Figure 5) it is only 91% charge transfer in character with 8.4% NAP-based transition (the same transition that dominates the NAP-based bright state). The stronger mixing in **2a** is due to a closer energy match between the pure NAP-based bright state and the pure CS state. These calculations support the observations that $\nu_{C\equiv C}$ (CS state) and $\nu_{C=O}(NAP^-)$ peaks are much stronger in **2d** than in **2a** (Table S4). The larger extent of CS state formation in **2d** compared to **2a** explains the larger red shift of its $\nu_{C\equiv C}$ band (Figure 8b). The $\nu_{C=O}(NAP^-)$ peaks of **2d** are also more red-shifted than those of **2a** (Figure 8a).

The spectral dynamics are different for **2a** and **2d**. For **2d**, formation of the CS state is time-resolved in the visible and IR regions, manifesting as rising components with different spectral shapes compared to those of the bright excited state

DOI: 10.1021/acs.inorgchem.9b02557
Inorg. Chem. 2019, 58, 15487−15497

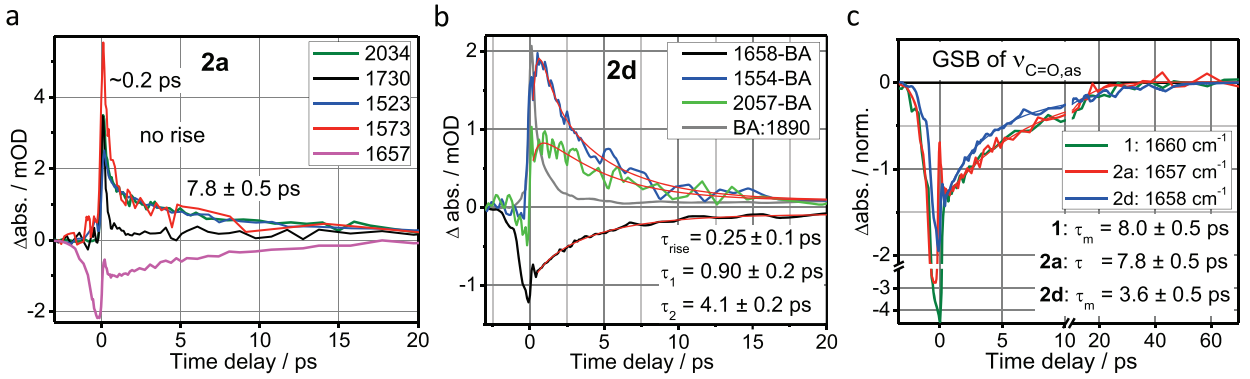

Figure 10. Transient kinetics for **2a** (a) and **2d** (b) at indicated frequencies (in cm^{-1}), normalized in (a) to show a match in characteristic decay times. The decay times of characteristic components are indicated on the graphs. (b) Global fit results are shown with red lines. (c) Normalized transient $\nu_{C=O,as}$ kinetics for **1**, **2a**, and **2d** at indicated frequencies (thick lines) and their fits with two-exponential functions (thin lines of matching colors). (inset) Mean decay times; the fit parameters are **1**: 3.6 ± 1.5 ps (40%) and 10.9 ± 2.4 ps (60%); **2a**: 7.8 ± 0.5 ps; **2d**: 0.9 ± 0.2 ps (17%) 4.1 ± 0.2 ps (83%).

prepared with a 400 nm pump. The rising components are most pronounced in the visible region (Figure 9b) and for the 1570 cm^{-1} peak (Figure 10b). The decay-associated spectral (DAS) analysis allows identification of the principle decay components common for kinetics at all wavelengths.[44,45] The DAS analysis of the early time dynamics for **2d** resulted in three sizable principal components, one rising and two decaying (Figure 9b). The DAS spectra of the rising (0.25 ± 0.05 ps) and first decaying (0.83 ± 0.1 ps) components are similar, suggesting rapid formation of a new state with dominating absorbance followed by its decay. The DAS spectrum of the slower decay component (3.6 ± 0.4 ps) is broad, resulting in a red shift of the spectrum. The two decay times are similar to the decay times of the C═O bleach peak decays and are associated with formation of a LLS (Figure 10c), suggesting that no other electronic excited states are formed.

In **2a** the visible decay-associated spectra for early time dynamics resulted in two principal decay components (Figure 9a); the two components, 0.68 and 7.7 ps, with similar DAS spectra indicate that both belong to the same species, while the state dynamics is not single exponential. It is conceivable that the formation of the CS state in **2a** occurs faster than the instrumental time resolution (<100 fs). This hypothesis is supported by TD-DFT analysis that shows mixing of the CS state and pure bright states in **2a**, which is expected to facilitate the electronic transition (Figure 5).

The vibronic dynamics in the mid-IR region is masked by a broad featureless absorbance across the fingerprint region, observed in all three compounds (Figure 8b and Figures S8 and S9). Such broad absorbance, reported previously for Pt-bis-alkynyl-NAP compounds, was attributed to transitions between closely spaced electronic states.[46−51] In **1** and **2a**, the broad absorption decays rapidly (0.1−0.2 ps, Figure S8), not preventing the assignment of the vibrational peaks. However, in **2d** the broad absorption (BA), in addition to a fast component of ca. 0.2 ps, features a relatively slow component of ca. 1.0 ps (Figures S9 and 10b), which significantly masks the dynamics on this same time scale (0.8 and 4 ps, Figure 9b). The broad featureless spectrum has a uniform amplitude across the 1680−2120 cm^{-1} region (Figure S9), which permits its subtraction from the signals at frequencies of characteristic vibrational transitions (C═O GSB, 1670 cm^{-1}, and at 2000−2100 cm^{-1}, Figure 10b). A global fit of the resulting kinetics produces the 0.25 ± 0.1 ps rise, 0.9 ± 0.2 ps, and 4.1 ± 0.2 ps decay time constants (Figure 10b), which are similar to those obtained in the DAS analysis in the visible region (Figure 9b).

The spectral dynamics for **2a** in the mid-IR is much simpler than that for **2d** featuring only a broad ultrafast component with an 8 ps decay (Figure 10a). Because of the time constant separation, no broad background subtraction was necessary for **2a**.

The C≡C peaks of the CS state in **2a** and **2d** are extremely broad, likely because of the wide distribution of dihedral angles between the donor and acceptor planes (θ) in the ground electronic state, which affects the D-A coupling strength and the extent of mixing. It is expected that the coupling is stronger for more planar D-A conformations (small θ angle), resulting in a larger dipole moment for the CS state. The decay times for **2d** (with dominant components between 0.9 and 4 ps, Figures 9b and 10b) are attributed to the process leading to a nonpolarized bridge—a charge recombination (CR) process. It is apparent that the CR process is faster in the more planar conformations (Figure 8b), but the difference is not large. Note that the spectral diffusion associated with the θ angle change in the CS state is not expected to contribute at the time window of 5 ps in **2d** due to the relatively larger size of its donor moiety.

The C≡C peak in the CS state of **2a** decays slower than that for **2d** with the dominant component of ca. 8 ps, which matches its C═O GSB recovery time (Figure 10a). The C≡C peak shifts to slightly lower frequencies with time (Figure 8b). The shift can be associated with the solvation dynamics further stabilizing the CS state. The red shift may also be influenced by differences in the CR rates at different θ angles, such that the decay is slower for conformations with smaller θ angles having red-shifted peaks, but the contributions of different relaxation processes are difficult to specify.

As noted earlier, the antisymmetric C≡C stretching mode dominates the spectrum in the GS, as the two ethynyl arms are exposed to a similar charge environment with the unit positive charge at the Co center and close to zero charges at the donor and acceptor moieties. However, in the CS state, the ethynyl mode at the acceptor side dominates the spectrum as the mixing of the two C≡C modes is reduced. Our population DFT analysis indicates that the Co center still carries approximately a unit charge in the CS state, while the electron is transferred from the donor to the acceptor moieties making

DOI: 10.1021/acs.inorgchem.9b02557
Inorg. Chem. 2019, 58, 15487−15497

the ethynyl group at the acceptor side polarized much stronger than that at the donor side and resulting in its dominant contribution to the C≡C IR intensity (Table S4).

Solvation, vibrational relaxation, and structural relaxation each complicate the dynamics, producing variations in kinetics at individual wavelengths. The following scheme (Scheme 2) is consistent with all major spectroscopic observations.

Scheme 2. Summary of the Excited-State Dynamics in 1, 2a, and 2d[a]

$$\mathbf{1}: \quad GS \xrightarrow{400\ nm} {}^1NAP \xrightarrow{8\ ps} {}^3Co(cyclam)$$

$$\mathbf{2a}: \quad GS \xrightarrow{400\ nm} {}^1NAP^{\&} \underset{CS}{\overset{<0.1\ ps}{\rightleftarrows}} {}^1CSS \xrightarrow[CR]{8\ ps} {}^3Co(cyclam)$$

$$\mathbf{2d}: \quad GS \xrightarrow{400\ nm} {}^1NAP^{\&} \underset{CS}{\overset{0.25\ ps}{\rightleftarrows}} {}^1CSS \xrightarrow[CR]{4\ ps} {}^3Co(cyclam)$$

[a] $^1NAP^{\&}$ denotes the NAP bright state with partial D(HOMO) → A(LUMO) contribution.

The long-lived state can be assigned to ^{3}Co(cyclam) or ^{3}NAP. TD-DFT analysis shows that the Co-based triplet state is lower in energy than the ^{3}NAP state (Figure S7). The vibrational frequencies of the NAP carbonyl modes were computed in both states. In the ^{3}Co(cyclam) state these frequencies differ from those in the GS by only a few wavenumbers, as observed experimentally. The C=O frequencies in a ^{3}NAP state were assessed in a fully organic compound, Ph−C_4-NAP, showing formation of the ^{3}NAP state (Figure S10, bottom panel). The C=O frequencies in the ^{3}NAP state are found to be ca. 50 cm^{-1} lower than the respective GS frequencies. Characteristic C=O frequencies for the ^{3}NAP state were reported at 1590, 1640, and 1950 cm^{-1} by Weinstein and co-workers.[8,43,46,52] The absence of significant peaks at these frequencies in the transient IR absorption spectra of **2a** and **2d** (Figure 8) eliminates the possibility of the ^{3}NAP state being the LLS and corroborates the assignment of ^{3}Co(cyclam). The presence of low-lying Co-based triplet and quintet states were found previously.[32] The Co-based quintet ($^5T_1$) state in $[Co(III)(en)_3](ClO_4)_3$ (en = ethylenediamine) was reported at energies below 900 nm.[34] Therefore, the LLS was assigned as the ^{3}Co(cyclam) state.

Since the fluorescence spectra of all three compounds are similar, one may expect to see the emission quantum yield in **2d** to be smaller than that in **1** by a factor of $k_{ISC}(\mathbf{1})/k_{CS}(\mathbf{2d})$, an approximate ratio of 31 (ISC = intersystem crossing). When excited at 400 nm, the measured emission quantum yield in **2d**, relative to that of **1**, is only 11-fold smaller. This discrepancy may originate from several factors such as the error for the determined rates, nonexponentiality of the excited state dynamics, and the possibility of exciting the donor moiety in the fluorescence measurements (which could result in a higher emission quantum yield). For example, just taking into account the error bars for the rates, the $k_{ISC}(\mathbf{1})/k_{CS}(\mathbf{2d})$ ratio could span from 21 to 37.

In the D-B-A dyads studied by Weinstein and co-workers, the deactivating d-d state lies significantly above the π^*(NAP) orbital, enabling a long-lived CS state ($\tau \approx 800$ ps), which in turn allows for the application of the second vibrational pump.[8,43,46,52] In the Co(cyclam) system, the deactivating d-d state is energetically below the π^*(NAP) orbital as evidenced by the $\lambda_{max}(^1A_1 \rightarrow {}^1T_1)$ being 480 nm in **1**, while that of $\pi-\pi^*(NAP^{iPr})$ is 400 nm, which led to short-lived CS state ($\tau \approx$ few ps). Note that ES lifetimes of typical Fe(II) complexes, isoelectronic with Co(III), are even shorter and often in sub-picoseconds.[53] Nonetheless, the use of strongly σ-donating terpyridine analogues led to the increase in the extent of metal-to-ligand charge transfer (MLCT) state, restricting the decay rate-determining step to the $^3T_1$ ($(t_{2g})^5(e_g^*)^1$) → $^1A_1$ ($(t_{2g})^6$) relaxation instead of $^5T_2$ ($(t_{2g})^4(e_g^*)^2$) → $^1A_1$, and thus resulting in very long lifetime of the excited states (550 ps).[54] With benzimidazolylidene-based ligands, the deactivating d-d state of Fe(II) complexes were significantly elevated, and the lifetimes of ^{3}MLCT were extended to a 100 ps level, making these types of complexes viable photosensitizers.[55,56] It is conceivable that the Co(III)-centered $^1T_1$ and $^3T_1$ state can be significantly destabilized by further enhancement of the ligand field strength, leading to the desired long-lived CS state.

CONCLUSIONS

Through stepwise addition of alkynyls, dissymmetric Co(III) D-B-A complexes were obtained in respectable yields, enabling the probe of excited-state CS dynamics. Despite the presence of Co-based triplet states at lower energies, efficient CS occurs in compounds **2a** and **2d**. The fast CS is enabled by strong communication between the donor and acceptor mediated by the Co(cyclam) bis-alkynyl bridge. The low-lying Co-based states eventually serve as energy sinks, resulting in CR. The Co-centered excited state is very long-lived, relaxing to the GS with a characteristic time of 2−4 ns. The CS-to-CR rate ratios are 16-fold for **2d** (0.25 ps/4 ps)$^{-1}$ and 80-fold for **2a** (0.1 ps/8 ps)$^{-1}$. Further CS studies involving more complex donors and/or acceptors are ongoing. If the CS in such systems remains efficient, the overall ET yield will remain high.

The D-B-A structures synthesized and studied here are appealing for future studies of IR-induced rate modulation. When the ET reaction is slower than the lifetime of the vibrational mode targeted for ET rate modulation, the relaxation of the vibrational mode during the ET reaction makes it difficult to ascertain the origin of the ET modulation, to either the excited vibrational mode or the daughter modes of its relaxation. When the ET reaction is fast, limited vibrational relaxation occurs during the ET reaction. The CS rate in **2d** is expected to be faster than the vibrational relaxation, making **2d** an attractive target for the ET modulation studies. The CR reaction, although slower than the vibrational relaxation, is still fast enough to include only a few daughter modes into analysis. The alkyne bridges offer substantial interactions among the D, B, and A moieties, suggesting that IR excitation of the bridge modes could strongly influence interactions among the subunits and thus perturb the ET kinetics. This hypothesis will be explored in future studies.

EXPERIMENTAL SECTION

Synthesis. General synthetic and analytical details are provided in the Supporting Information. A brief description of the *unique* syntheses is provided here.

Synthesis of [Co(cyclam)(C_2NAP^{iPr})Cl]Cl (1). $[Co(cyclam)Cl_2]Cl$ (0.76 mmol) was dissolved in 50 mL of CH_3OH, to which a 20 mL solution of tetrahydrofuran (THF) containing 4-ethynyl-*N*-isopropyl-1,8-naphthalimide (0.91 mmol) was added and purged with N_2. With addition of Et_3N (2.0 mL, 15 mmol) the solution darkened and then refluxed for 16 h. Silica plug purification with CH_3OH/CH_2Cl_2 (v/v, 1:6) eluted the product as an orange band. Recrystallization from methanol and ether yielded 392 mg of **1** as an orange solid (87% based on $[Co(cyclam)Cl_2]Cl$). Single crystals of **1** were obtained

DOI: 10.1021/acs.inorgchem.9b02557
Inorg. Chem. 2019, 58, 15487−15497

from the slow diffusion of hexanes/ether (v/v, 1:2) into CH_3OH containing **1**.

Synthesis of [Co(cyclam)(C_2NAP^{iPr})($C_2C_6H_4$-4-NMe_2)]Cl (2a). Compound **1** (0.23 mmol) was dried under vacuum. Lithiated 4-ethynyl-*N*,*N*-dimethylaniline (40 mg, 0.28 mmol) was added via cannula while stirring at −78 °C. The solution turned dark red and was allowed to slowly warm to room temperature over a period of 8 h. The resulting dark orange solution was purified over silica. The desired product eluted as a yellow band with CH_3OH/CH_2Cl_2(v/v, 1:6). Recrystallization from methanol and ether yielded 81 mg of **2a** (50% based on **1**). Single crystals of **2a** were grown from slow diffusion of hexanes/ether (v/v, 1:1) into a CH_2Cl_2/CH_3OH (v/v, 1:1) solution containing **2a**.

Synthesis of [Co(cyclam)(C_2NAP^{iPr})$_2$]Cl (2b). To a 20 mL THF solution containing LiC_2NAP^{iPr} (77 mg, 0.29 mmol) was added vacuum-dried **1** (100 mg, 0.17 mmol). The dark red solution was stirred at −78 °C for 4 h and then quenched with air. Upon solvent removal, the residue was purified by column chromatography (SiO_2, CH_3OH/CH_2Cl_2 v/v, 1:6) and eluted as a yellow band. The product was then rinsed with CH_3OH, and the filtrate was collected and recrystallized from CH_2Cl_2 and ether to yield 57 mg of **2b** as a yellow solid (37% based on **1**).

Synthesis of [Co(cyclam)(C_2NAP^{iPr})($C_2C_6H_4$-4-N(Ph-4′-OMe)$_2$]Cl (2d). A 100 mL Schlenk tube was charged with 46 mg (0.08 mmol) of **1** and dried under vacuum, and an 8 mL THF solution of LiC_2TPA (0.16 mmol) was added while stirring at −78 °C, turning the solution bright red. The solution was allowed to stir for 3 h, and then the reaction was quenched with CH_3OH. Solvent was removed, and the crude residue was purified by column chromatography (SiO_2, CH_3OH/CH_2Cl_2 v/v, 1:6), eluting as an orange band, and recrystallized from CH_2Cl_2/hexanes to yield 13 mg of orange solid (19% based on **1**).

Ultrafast Dynamics and TR-IR Details. The three-pulse transient absorption setup, capable of detecting transient spectra in the vis/near-IR or mid-IR spectral regions, is based on a Ti:sapphire oscillator−regenerative amplifier tandem (Vitesse from Coherent and Spitfire from Spectra Physics). The output laser beam (1.1 mJ pulse energy, 1 kHz repetition rate, 804 nm wavelength, and 44 fs pulse duration) was split into three parts. One part of ca. 370 μJ/pulse was frequency doubled to generate 402 nm excitation pulses, providing 1−2 μJ/pulse for these experiments. The second part of ca. 630 μJ/pulse was used to generate mid-IR pluses of ca. 200 cm^{-1} spectral width (full width at half-maximum (fwhm)) frequency tunable from 1000 to 4000 cm^{-1} via an in-house-built optical parametric amplifier and difference frequency generation units. The third part (ca. 7 μJ/pulse) was intensity-tuned by a wave plate-polarizer pair and focused into a sapphire wafer to generate white light continuum. All three beams overlapped in the sample, but either visible/near-IR or mid-IR probe beam was used in the experiments. Transient spectra in the visible region were measured with a charge coupled device (CCD) camera (PIXIS-100, Princeton Instrument) attached to a monochromator (TRIAX-190, Horiba); the mid-IR spectra were detected with a single-channel mercury cadmium telluride (MCT) detector (Infrared Associates). The experiments were performed in a flow cell of 100 μm path length at room temperature (22 ± 0.5 °C).

Computational Details. DFT and TD-DFT calculations for the cations in **1**, **2a**, and **2d** were performed using the MN15 functional[57] and the Def2-SVP basis set[58] for all atoms as implemented in Gaussian 16.[59] The Polarizable Continuum Model (PCM)[60] was used to simulate the solvent effects of acetonitrile in the ground-state and excited-state calculations. The B3LYP, CAM-B3LYP, wB97X-D, M06, and M06-2X functionals were also tested by comparing the character of the excited states and the vertical excitation energies with experiments. A better agreement with the experimental vibrational frequencies and electronic spectra was found with the MN15 functional. Coordinates of the optimized geometries in the ground state are listed in Tables S5−S7.

■ ASSOCIATED CONTENT

Supporting Information

The Supporting Information is available free of charge on the ACS Publications website at DOI: 10.1021/acs.inorgchem.9b02557.

Synthesis and characterization details, absorption of free ligands, electrochemical data (vs $Ag/AgNO_3$), crystallographic details, IR kinetics, TR-IR of PhC_4NAp^{iPr}, TD-DFT results, and DFT coordinates of optimized structures (PDF)

Accession Codes

CCDC 1941901−1941902 contain the supplementary crystallographic data for this paper. These data can be obtained free of charge via www.ccdc.cam.ac.uk/data_request/cif, or by emailing data_request@ccdc.cam.ac.uk, or by contacting The Cambridge Crystallographic Data Centre, 12 Union Road, Cambridge CB2 1EZ, UK; fax: +44 1223 336033.

■ AUTHOR INFORMATION

Corresponding Authors

*E-mail: tren@purdue.edu. (T.R.)
*E-mail: irubtsov@tulane.edu. (I.V.R.)
*E-mail: david.beratan@duke.edu. (D.N.B.)

ORCID

Matthias Zeller: 0000-0002-3305-852X
David N. Beratan: 0000-0003-4758-8676
Igor V. Rubtsov: 0000-0002-3010-6207
Tong Ren: 0000-0002-1148-0746

Author Contributions

#These authors contribute equally.

Notes

The authors declare no competing financial interest.

■ ACKNOWLEDGMENTS

We thank the National Science Foundation for generously supporting this work (CHE-1764347 to T.R. at Purdue, CHE-1565427 to I.V.R. at Tulane, CHE-1565812 to D.N.B. at Duke, and CHE-1625543 for X-ray diffractometers at Purdue). S.D.B. thanks Purdue University for a Cagiantas Fellowship. J.V. gratefully acknowledges support of a Fulbright-Garcia Robles Scholarship and a Graduate Program in Nanoscience (GP-Nano) Fellowship from Duke Univ.

■ REFERENCES

(1) Albinsson, B.; Mårtensson, J. Long-range electron and excitation energy transfer in donor−bridge−acceptor systems. *J. Photochem. Photobiol., C* **2008**, *9*, 138−155.

(2) Barbara, P. F.; Meyer, T. J.; Ratner, M. A. Contemporary Issues in Electron Transfer Research. *J. Phys. Chem.* **1996**, *100*, 13148−13168.

(3) Lin, Z. W.; Lawrence, C. M.; Xiao, D. Q.; Kireev, V. V.; Skourtis, S. S.; Sessler, J. L.; Beratan, D. N.; Rubtsov, I. V. Modulating Unimolecular Charge Transfer by Exciting Bridge Vibrations. *J. Am. Chem. Soc.* **2009**, *131*, 18060−18062.

(4) Ma, Z.; Lin, Z. W.; Lawrence, C.; Rubtsov, I. V.; Antoniou, P.; Skourtis, S. S.; Zhang, P.; Beratan, D. N. How can infra-red excitation both accelerate and slow charge transfer in the same molecule? *Chem. Sci.* **2018**, *9*, 6395−6405.

(5) Yue, Y. K.; Grusenmeyer, T.; Ma, Z.; Zhang, P.; Schmehl, R. H.; Beratan, D. N.; Rubtsov, I. V. Electron transfer rate modulation in a compact Re(I) donor-acceptor complex. *Dalton Trans* **2015**, *44*, 8609−8616.

DOI: 10.1021/acs.inorgchem.9b02557
Inorg. Chem. 2019, 58, 15487−15497

(6) Delor, M.; Scattergood, P. A.; Sazanovich, I. V.; Parker, A. W.; Greetham, G. M.; Meijer, A. J. H. M.; Towrie, M.; Weinstein, J. A. Toward control of electron transfer in donor-acceptor molecules by bond-specific infrared excitation. *Science* **2014**, *346*, 1492−1495.
(7) Delor, M.; Keane, T.; Scattergood, P. A.; Sazanovich, I. V.; Greetham, G. M.; Towrie, M.; Meijer, A. J. H. M.; Weinstein, J. A. On the mechanism of vibrational control of light-induced charge transfer in donor−bridge−acceptor assemblies. *Nat. Chem.* **2015**, *7*, 689−695.
(8) Scattergood, P. A.; Delor, M.; Sazanovich, I. V.; Bouganov, O. V.; Tikhomirov, S. A.; Stasheuski, A. S.; Parker, A. W.; Greetham, G. M.; Towrie, M.; Davies, E. S.; Meijer, A. J. H. M.; Weinstein, J. A. Electron transfer dynamics and excited state branching in a charge-transfer platinum(II) donor-bridge-acceptor assembly. *Dalton Trans* **2014**, *43*, 17677−17693.
(9) Rubtsov, I. V. STATE-SPECIFIC ELECTRON TRANSFER Shake it off. *Nat. Chem.* **2015**, *7*, 683−684.
(10) Haque, A.; Al-Balushi, R. A.; Al-Busaidi, I. J.; Khan, M. S.; Raithby, P. R. Rise of Conjugated Poly-ynes and Poly(Metalla-ynes): From Design Through Synthesis to Structure−Property Relationships and Applications. *Chem. Rev.* **2018**, *118*, 8474−8597.
(11) Bruce, M. I. Transition Metal Complexes Containing Allenylidene, Cumulenylidene, and Related Ligands. *Chem. Rev.* **1998**, *98*, 2797−858.
(12) Szafert, S.; Gladysz, J. A. Update 1 of: Carbon in One Dimension: Structural Analysis of the Higher Conjugated Polyynes. *Chem. Rev.* **2006**, *106*, 1−33.
(13) Pigulski, B.; Gulia, N.; Szafert, S. Reactivity of Polyynes: Complex Molecules from Simple Carbon Rods. *Eur. J. Org. Chem.* **2019**, *2019*, 1420−1445.
(14) Schull, T. L.; Kushmerick, J. G.; Patterson, C. H.; George, C.; Moore, M. H.; Pollack, S. K.; Shashidhar, R. Ligand Effects on Charge Transport in Platinum(II) Acetylides. *J. Am. Chem. Soc.* **2003**, *125*, 3202−3203.
(15) Blum, A. S.; Ren, T.; Parish, D. A.; Trammell, S. A.; Moore, M. H.; Kushmerick, J. G.; Xu, G.-L.; Deschamps, J. R.; Pollack, S. K.; Shashidhar, R. $Ru_2(ap)_4$((-oligo(phenyleneethynyl)) Molecular Wires: Synthesis and Electronic Characterization. *J. Am. Chem. Soc.* **2005**, *127*, 10010−10011.
(16) Meng, F. B.; Hervault, Y. M.; Norel, L.; Costuas, K.; Van Dyck, C.; Geskin, V.; Cornil, J.; Hng, H. H.; Rigaut, S.; Chen, X. D. Photo-modulable molecular transport junctions based on organometallic molecular wires. *Chem. Sci.* **2012**, *3*, 3113−3118.
(17) Tanaka, Y.; Kato, Y.; Tada, T.; Fujii, S.; Kiguchi, M.; Akita, M. Doping" of Polyyne with an Organometallic Fragment Leads to Highly Conductive Metallapolyyne Molecular Wire. *J. Am. Chem. Soc.* **2018**, *140*, 10080−10084.
(18) Meng, F. B.; Hervault, Y. M.; Shao, Q.; Hu, B. H.; Norel, L.; Rigaut, S.; Chen, X. D. Orthogonally modulated molecular transport junctions for resettable electronic logic gates. *Nat. Commun.*. **2014**, *5*, Art. 3023. DOI: 10.1038/ncomms4023
(19) Zhu, H.; Pookpanratana, S. J.; Bonevich, J. E.; Natoli, S. N.; Hacker, C. A.; Ren, T.; Suehle, J. S.; Richter, C. A.; Li, Q. Redox-Active Molecular Nanowire Flash Memory for High-Endurance and High-Density Non-Volatile Memory Applications. *ACS Appl. Mater. Interfaces* **2015**, *7*, 27306−27313.
(20) Wong, W.-Y.; Ho, C.-L. Organometallic Photovoltaics: A New and Versatile Approach for Harvesting Solar Energy Using Conjugated Polymetallaynes. *Acc. Chem. Res.* **2010**, *43*, 1246−1256.
(21) Ho, C.-L.; Yu, Z.-Q.; Wong, W.-Y. Multifunctional poly-metallaynes: properties, functions and applications. *Chem. Soc. Rev.* **2016**, *45*, 5264−5295.
(22) Bhaskar, A.; Ramakrishna, G.; Lu, Z. K.; Twieg, R.; Hales, J. M.; Hagan, D. J.; Van Stryland, E.; Goodson, T. Investigation of two-photon absorption properties in branched alkene and alkyne chromophores. *J. Am. Chem. Soc.* **2006**, *128*, 11840−11849.
(23) Williams-Harry, M.; Bhaskar, A.; Ramakrishna, G.; Goodson, T.; Imamura, M.; Mawatari, A.; Nakao, K.; Enozawa, H.; Nishinaga, T.; Iyoda, M. Giant thienylene-acetylene-ethylene macrocycles with large two-photon absorption cross section and semishape-persistence. *J. Am. Chem. Soc.* **2008**, *130*, 3252−3253.
(24) Ren, T. A Sustainable Metal Alkynyl Chemistry: 3d Metals and Polyaza Macrocyclic Ligands. *Chem. Commun.* **2016**, *52*, 3271−3279.
(25) Banziger, S. D.; Ren, T. Syntheses, Structures and Bonding of 3d Metal Alkynyl Complexes of Cyclam and Its Derivatives. *J. Organomet. Chem.* **2019**, *885*, 39−48.
(26) Hoffert, W. A.; Kabir, M. K.; Hill, E. A.; Mueller, S. M.; Shores, M. P. Stepwise acetylide ligand substitution for the assembly of ethynylbenzene-linked Co(III) complexes. *Inorg. Chim. Acta* **2012**, *380*, 174−180.
(27) Cook, T. D.; Natoli, S. N.; Fanwick, P. E.; Ren, T. Dimeric Complexes of CoIII(cyclam) with a Polyynediyl Bridge. *Organo-metallics* **2015**, *34*, 686−689.
(28) Cook, T. D.; Natoli, S. N.; Fanwick, P. E.; Ren, T. CoIII(cyclam) Oligoynyls: Monomeric Oligoynyl Complexes and Dimeric Complexes with an Oligoyn-diyl Bridge. *Organometallics* **2016**, *35*, 1329−1338.
(29) Natoli, S. N.; Zeller, M.; Ren, T. Stepwise Synthesis of Bis-Alkynyl CoIII(cyclam) Complexes under Ambient Conditions. *Inorg. Chem.* **2016**, *55*, 5756−5758.
(30) Natoli, S. N.; Zeller, M.; Ren, T. An Aerobic Synthetic Approach Toward Bis-Alkynyl Cobalt(III) Compounds. *Inorg. Chem.* **2017**, *56*, 10021−10031.
(31) Banziger, S. D.; Cook, T. D.; Natoli, S. N.; Fanwick, P. E.; Ren, T. Synthetic and Structural Studies of Mono-acetylide and Unsymmetric Bis-acetylide Complexes based on CoIII-cyclam. *J. Organomet. Chem.* **2015**, *799*−*800*, 1−6.
(32) Rury, A. S.; Wiley, T. E.; Sension, R. J. Energy Cascades, Excited State Dynamics, and Photochemistry in Cob(III)alamins and Ferric Porphyrins. *Acc. Chem. Res.* **2015**, *48*, 860−867.
(33) Miller, N. A.; Wiley, T. E.; Spears, K. G.; Ruetz, M.; Kieninger, C.; Krautler, B.; Sension, R. J. Toward the Design of Photoresponsive Conditional Antivitamins B-12: A Transient Absorption Study of an Arylcobalamin and an Alkynylcobalamin. *J. Am. Chem. Soc.* **2016**, *138*, 14250−14256.
(34) McCusker, J. K.; Walda, K. N.; Magde, D.; Hendrickson, D. N. Picosecond Excited-State Dynamics in Octahedral Cobalt(Iii) Complexes - Intersystem Crossing Versus Internal-Conversion. *Inorg. Chem.* **1993**, *32*, 394−399.
(35) Pal, A. K.; Li, C. F.; Hanan, G. S.; Zysman-Colman, E. Blue-Emissive Cobalt(III) Complexes and Their Use in the Photocatalytic Trifluoromethylation of Polycyclic Aromatic Hydrocarbons. *Angew. Chem., Int. Ed.* **2018**, *57*, 8027−8031.
(36) Langford, C. H.; Malkhasian, A. Y. S.; Sharma, D. K. Subnanosecond Transients in the Spectra of Cobalt(Iii) Amine Complexes. *J. Am. Chem. Soc.* **1984**, *106*, 2727−2728.
(37) Banziger, S. D.; Judkins, E. C.; Zeller, M.; Ren, T. Diruthenium-DMBA Bis-Alkynyl Compounds with Hetero- and Extended- Aryl Appendant. *Chin. J. Inorg. Chem.* **2017**, *33*, 2103−2109.
(38) Heyer, E.; Ziessel, R. Panchromatic Push-Pull Dyes of Elongated Form from Triphenylamine, Diketopyrrolopyrrole, and Tetracyanobutadiene Modules. *Synlett* **2015**, *26*, 2109−2116.
(39) Long, N. J.; Williams, C. K. Metal Alkynyl Complexes: Synthesis and Materials. *Angew. Chem., Int. Ed.* **2003**, *42*, 2586−2617.
(40) Judkins, E. C.; Zeller, M.; Ren, T. Synthesis and Characterizations of Macrocyclic Cr(III) and Co(III) 1-Ethynyl Naphthalene and 9-Ethynyl Anthracene Complexes: An Investigation of Structural and Spectroscopic Properties. *Inorg. Chem.* **2018**, *57*, 2249−2259.
(41) Thakker, P. U.; Aru, R. G.; Sun, C.; Pennington, W. T.; Siegfried, A. M.; Marder, E. C.; Wagenknecht, P. S. Synthesis of trans bis-alkynyl complexes of Co(III) supported by a tetradentate macrocyclic amine: A spectroscopic, structural, and electrochemical analysis of pi-interactions and electronic communication in the C equivalent to C-M-C equivalent to C structural unit. *Inorg. Chim. Acta* **2014**, *411*, 158−164.
(42) McAdam, C. J.; Morgan, J. L.; Robinson, B. H.; Simpson, J.; Rieger, P. H.; Rieger, A. L. Tunable Donora−Acceptor Interactions in

DOI: 10.1021/acs.inorgchem.9b02557
Inorg. Chem. 2019, 58, 15487−15497

4-Ene/Yne-Ferrocenyl and 4-Enamine Naphthalimides with Ferrocenyl Headgroups. *Organometallics* **2003**, *22*, 5126−5136.
(43) Sazanovich, I. V.; Alamiry, M. A. H.; Best, J.; Bennett, R. D.; Bouganov, O. V.; Davies, E. S.; Grivin, V. P.; Meijer, A.; Plyusnin, V. F.; Ronayne, K. L.; Shelton, A. H.; Tikhomirov, S. A.; Towrie, M.; Weinstein, J. A. Excited State Dynamics of a Pt-II Diimine Complex bearing a Naphthalene-Diimide Electron Acceptor. *Inorg. Chem.* **2008**, *47*, 10432−10445.
(44) Knutson, J. R.; Walbridge, D. G.; Brand, L. Decay-Associated Fluorescence-Spectra and the Heterogeneous Emission of Alcohol-Dehydrogenase. *Biochemistry* **1982**, *21*, 4671−4679.
(45) van Stokkum, I. H. M.; Larsen, D. S.; van Grondelle, R. Global and target analysis of time-resolved spectra. *Biochim. Biophys. Acta, Bioenerg.* **2004**, *1657*, 82−104.
(46) Sazanovich, I. V.; Best, J.; Scattergood, P. A.; Towrie, M.; Tikhomirov, S. A.; Bouganov, O. V.; Meijer, A.; Weinstein, J. A. Ultrafast photoinduced charge transport in Pt(II) donor-acceptor assembly bearing naphthalimide electron acceptor and phenothiazine electron donor. *Phys. Chem. Chem. Phys.* **2014**, *16*, 25775−25788.
(47) Castellano, F. N. Transition metal complexes meet the rylenes. *Dalton Trans* **2012**, *41*, 8493−8501.
(48) Dixon, D. W.; Thornton, N. B.; Steullet, V.; Netzel, T. Effect of DNA scaffolding on intramolecular electron transfer quenching of a photoexcited ruthenium(II) polypyridine naphthalene diimide. *Inorg. Chem.* **1999**, *38*, 5526−5534.
(49) Johansson, O.; Wolpher, H.; Borgstrom, M.; Hammarstrom, L.; Bergquist, J.; Sun, L. C.; Akermark, B. Intramolecular charge separation in a hydrogen bonded tyrosine-ruthenium(II)-naphthalene diimide triad. *Chem. Commun.* **2004**, 194−195.
(50) McAdam, C. J.; Manning, A. R.; Robinson, B. H.; Simpson, J. Group 8 and 10 metal acetylide naphthalimide dyads. *Inorg. Chim. Acta* **2005**, *358*, 1673−1682.
(51) Prodi, A.; Chiorboli, C.; Scandola, F.; Iengo, E.; Alessio, E.; Dobrawa, R.; Wurthner, F. Wavelength-dependent electron and energy transfer pathways in a side-to-face ruthenium porphyrin/perylene bisimide assembly. *J. Am. Chem. Soc.* **2005**, *127*, 1454−1462.
(52) Sazanovich, I. V.; Alamiry, M. A. H.; Meijer, A.; Towrie, M.; Davies, E. S.; Bennett, R. D.; Weinstein, J. A. Photoinduced charge separation in a Pt-II acetylide donor-acceptor triad based on 2-(1-pyrazole)-pyridine modified with naphthalene mono-imide electron acceptor. *Pure Appl. Chem.* **2013**, *85*, 1331−1348.
(53) Monat, J. E.; McCusker, J. K. Femtosecond excited-state dynamics of an iron(II) polypyridyl solar cell sensitizer model. *J. Am. Chem. Soc.* **2000**, *122*, 4092−4097.
(54) Mengel, A. K. C.; Forster, C.; Breivogel, A.; Mack, K.; Ochsmann, J. R.; Laquai, F.; Ksenofontov, V.; Heinze, K. A Heteroleptic Push-Pull Substituted Iron(II) Bis(tridentate) Complex with Low-Energy Charge-Transfer States. *Chem. - Eur. J.* **2015**, *21*, 704−714.
(55) Liu, L.; Duchanois, T.; Etienne, T.; Monari, A.; Beley, M.; Assfeld, X.; Haacke, S.; Gros, P. C. A new record excited state (MLCT)-M-3 lifetime for metalorganic iron(II) complexes. *Phys. Chem. Chem. Phys.* **2016**, *18*, 12550−12556.
(56) Harlang, T. C. B.; Liu, Y. Z.; Gordivska, O.; Fredin, L. A.; Ponseca, C. S.; Huang, P.; Chabera, P.; Kjaer, K. S.; Mateos, H.; Uhlig, J.; Lomoth, R.; Wallenberg, R.; Styring, S.; Persson, P.; Sundstrom, V.; Warnmark, K. Iron sensitizer converts light to electrons with 92% yield. *Nat. Chem.* **2015**, *7*, 883−889.
(57) Yu, H. Y. S.; He, X.; Li, S. H. L.; Truhlar, D. G. MN15: A Kohn-Sham global-hybrid exchange-correlation density functional with broad accuracy for multi-reference and single-reference systems and noncovalent interactions. *Chem. Sci.* **2016**, *7*, 5032−5051.
(58) Weigend, F.; Ahlrichs, R. Balanced basis sets of split valence, triple zeta valence and quadruple zeta valence quality for H to Rn: Design and assessment of accuracy. *Phys. Chem. Chem. Phys.* **2005**, *7*, 3297−3305.
(59) Frisch, M. J.; Trucks, G. W.; Schlegel, H. B.; Scuseria, G. E.; Robb, M. A.; Cheeseman, J. R.; Scalmani, G.; Barone, V.; Petersson, G. A.; Nakatsuji, H.; Li, X.; Caricato, M.; Marenich, A. V.; Bloino, J.; Janesko, B. G.; Gomperts, R.; Mennucci, B.; Hratchian, H. P.; Ortiz, J. V.; Izmaylov, A. F.; Sonnenberg, J. L.; Williams; Ding, F.; Lipparini, F.; Egidi, F.; Goings, J.; Peng, B.; Petrone, A.; Henderson, T.; Ranasinghe, D.; Zakrzewski, V. G.; Gao, J.; Rega, N.; Zheng, G.; Liang, W.; Hada, M.; Ehara, M.; Toyota, K.; Fukuda, R.; Hasegawa, J.; Ishida, M.; Nakajima, T.; Honda, Y.; Kitao, O.; Nakai, H.; Vreven, T.; Throssell, K.; Montgomery, J. A., Jr.; Peralta, J. E.; Ogliaro, F.; Bearpark, M. J.; Heyd, J. J.; Brothers, E. N.; Kudin, K. N.; Staroverov, V. N.; Keith, T. A.; Kobayashi, R.; Normand, J.; Raghavachari, K.; Rendell, A. P.; Burant, J. C.; Iyengar, S. S.; Tomasi, J.; Cossi, M.; Millam, J. M.; Klene, M.; Adamo, C.; Cammi, R.; Ochterski, J. W.; Martin, R. L.; Morokuma, K.; Farkas, O.; Foresman, J. B.; Fox, D. J. *Gaussian 16*, Rev. B.01; Gaussian, Inc.: Wallingford, CT, 2016.
(60) Scalmani, G.; Frisch, M. J. Continuous surface charge polarizable continuum models of solvation. I. General formalism. *J. Chem. Phys.* **2010**, *132*, 114110.

DOI: 10.1021/acs.inorgchem.9b02557
Inorg. Chem. 2019, 58, 15487−15497